

A Precise Measurement of the Neutron Magnetic Form Factor G_M^n in the Few-GeV² Region

J. Lachniet,^{1,2} A. Afanasev,³ H. Arenhövel,⁴ W.K. Brooks,⁵ G.P. Gilfoyle,⁶ S. Jeschonnek,⁷
B. Quinn,¹ M.F. Vineyard,⁸ G. Adams,³⁶ K. P. Adhikari,² M.J. Amarian,²
M. Anghinolfi,²⁵ B. Asavapibhop,³¹ G. Asryan,⁴⁴ H. Avakian,^{24,40} H. Bagdasaryan,²
N. Baillie,⁴³ J.P. Ball,¹⁰ N.A. Baltzell,³⁹ S. Barrow,²⁰ V. Batourine,^{40,*} M. Battaglieri,²⁵
K. Beard,²⁸ I. Bedlinskiy,²⁷ M. Bektasoglu,^{2,†} M. Bellis,¹ N. Benmouna,²¹ B.L. Berman,²¹
A.S. Biselli,¹⁸ B.E. Bonner,³⁷ C. Bookwalter,²⁰ S. Bouchigny,^{40,26} S. Boiarinov,^{27,40}
R. Bradford,¹ D. Branford,¹⁷ W.J. Briscoe,²¹ S. Bültmann,² V.D. Burkert,⁴⁰
J.R. Calarco,³² S.L. Careccia,² D.S. Carman,⁴⁰ L. Casey,¹³ L. Cheng,¹³ P.L. Cole,^{40,23}
A. Coleman,^{43,‡} P. Collins,¹⁰ D. Cords,⁴⁰ P. Corvisiero,²⁵ D. Crabb,⁴² V. Crede,²⁰
J.P. Cummings,³⁶ D. Dale,²³ A. Daniel,³⁴ N. Dashyan,⁴⁴ R. De Masi,¹⁴ R. De Vita,²⁵
E. De Sanctis,²⁴ P.V. Degtyarenko,⁴⁰ H. Denizli,³⁵ L. Dennis,²⁰ A. Deur,⁴⁰ S. Dhamija,¹⁹
K.V. Dharmawardane,² K.S. Dhuga,²¹ R. Dickson,¹ C. Djalali,³⁹ G.E. Dodge,²
D. Doughty,^{15,40} P. Dragovitsch,²⁰ M. Dugger,¹⁰ S. Dytman,³⁵ O.P. Dzyubak,³⁹
H. Egiyan,^{43,32} K.S. Egiyan,⁴⁴ L. El Fassi,⁹ L. Elouadrhiri,^{15,40} A. Empl,³⁶ P. Eugenio,²⁰
R. Fatemi,⁴² G. Fedotov,³⁸ R. Fersch,⁴³ R.J. Feuerbach,¹ T.A. Forest,^{2,23} A. Fradi,²⁶
M.Y. Gabrielyan,¹⁹ M. Garçon,¹⁴ G. Gavalian,^{32,2} N. Gevorgyan,⁴⁴ K.L. Giovanetti,²⁸
F.X. Girod,^{14,§} J.T. Goetz,¹¹ W. Gohn,¹⁶ E. Golovatch,^{25,38} R.W. Gothe,³⁹ L. Graham,³⁹
K.A. Griffioen,⁴³ M. Guidal,²⁶ M. Guillo,³⁹ N. Guler,² L. Guo,^{40,¶} V. Gyurjyan,⁴⁰
C. Hadjidakis,²⁶ K. Hafidi,⁹ H. Hakobyan,⁴⁴ C. Hanretty,²⁰ J. Hardie,^{15,40} N. Hassall,²²
D. Heddle,^{15,40} F.W. Hersman,³² K. Hicks,³⁴ I. Hleiqawi,³⁴ M. Holtrop,³² J. Hu,³⁶
M. Huertas,³⁹ C.E. Hyde-Wright,² Y. Ilieva,³⁹ D.G. Ireland,²² B.S. Ishkhanov,³⁸
E.L. Isupov,³⁸ M.M. Ito,⁴⁰ D. Jenkins,⁴¹ H.S. Jo,²⁶ J.R. Johnstone,²² K. Joo,^{42,16}
H.G. Juengst,^{2,**} T. Kageya,⁴⁰ N. Kalantarians,² D. Keller,³⁴ J.D. Kellie,²²
M. Khandaker,³³ P. Khetarpal,³⁶ K.Y. Kim,³⁵ K. Kim,²⁹ W. Kim,²⁹ A. Klein,²
F.J. Klein,^{40,19,13} M. Klusman,³⁶ P. Konczykowski,¹⁴ M. Kossov,²⁷ L.H. Kramer,^{19,40}
V. Kubarovsky,⁴⁰ J. Kuhn,¹ S.E. Kuhn,² S.V. Kuleshov,²⁷ V. Kuznetsov,²⁹ J.M. Laget,^{14,40}
J. Langheinrich,³⁹ D. Lawrence,³¹ A.C.S. Lima,²¹ K. Livingston,²² M. Lowry,⁴⁰ H.Y. Lu,³⁹
K. Lukashin,^{40,13} M. MacCormick,²⁶ S. Malace,³⁹ J.J. Manak,⁴⁰ N. Markov,¹⁶

P. Mattione,³⁷ S. McAleer,²⁰ M.E. McCracken,¹ B. McKinnon,²² J.W.C. McNabb,¹
 B.A. Mecking,⁴⁰ M.D. Mestayer,⁴⁰ C.A. Meyer,¹ T. Mibe,³⁴ K. Mikhailov,²⁷ T. Mineeva,¹⁶
 R. Minehart,⁴² M. Mirazita,²⁴ R. Miskimen,³¹ V. Mokeev,^{38,40} B. Moreno,²⁶ K. Moriya,¹
 S.A. Morrow,^{14,26} M. Moteabbed,¹⁹ J. Mueller,³⁵ E. Munevar,²¹ G.S. Mutchler,³⁷
 P. Nadel-Turonski,¹³ R. Nasseripour,^{19,39,†} S. Niccolai,^{21,26} G. Niculescu,^{34,28}
 I. Niculescu,^{21,28} B.B. Niczyporuk,⁴⁰ M.R. Niroula,² R.A. Niyazov,^{2,36} M. Nozar,⁴⁰
 G.V. O’Rielly,²¹ M. Osipenko,^{25,38} A.I. Ostrovidov,²⁰ K. Park,^{29,39} S. Park,²⁰ E. Pasyuk,¹⁰
 C. Paterson,²² S. Anefalos Pereira,²⁴ S.A. Philips,²¹ J. Pierce,⁴² N. Pivnyuk,²⁷ D. Pocanic,⁴²
 O. Pogorelko,²⁷ E. Polli,²⁴ I. Popa,²¹ S. Pozdniakov,²⁷ B.M. Freedom,³⁹ J.W. Price,¹²
 Y. Prok,^{42,‡} D. Protopopescu,^{32,22} L.M. Qin,² B.A. Raue,^{19,40} G. Riccardi,²⁰ G. Ricco,²⁵
 M. Ripani,²⁵ B.G. Ritchie,¹⁰ G. Rosner,²² P. Rossi,²⁴ D. Rowntree,³⁰ P.D. Rubin,^{6,45}
 F. Sabatié,^{2,14} M.S. Saini,²⁰ J. Salamanca,²³ C. Salgado,³³ A. Sandorfi,⁴⁰ J.P. Santoro,¹³
 V. Sapunenko,^{25,40} D. Schott,¹⁹ R.A. Schumacher,¹ V.S. Serov,²⁷ Y.G. Sharabian,⁴⁰
 D. Sharov,³⁸ J. Shaw,³¹ N.V. Shvedunov,³⁸ A.V. Skabelin,³⁰ E.S. Smith,⁴⁰ L.C. Smith,⁴²
 D.I. Sober,¹³ D. Sokhan,¹⁷ A. Starostin,¹¹ A. Stavinsky,²⁷ S. Stepanyan,^{40,44}
 S.S. Stepanyan,²⁹ B.E. Stokes,²¹ P. Stoler,³⁶ K. A. Stopani,³⁸ I.I. Strakovsky,²¹
 S. Strauch,³⁹ R. Suleiman,³⁰ M. Taiuti,²⁵ S. Taylor,³⁷ D.J. Tedeschi,³⁹ R. Thompson,³⁵
 A. Tkabladze,^{21,†} S. Tkachenko,² M. Ungaro,^{36,16} A.V. Vlassov,²⁷ D.P. Watts,^{22,§§}
 X. Wei,⁴⁰ L.B. Weinstein,² D.P. Weygand,⁴⁰ M. Williams,¹ E. Wolin,⁴⁰ M.H. Wood,³⁹
 A. Yegneswaran,⁴⁰ J. Yun,² M. Yurov,²⁹ L. Zana,³² J. Zhang,² B. Zhao,¹⁶ and Z.W. Zhao³⁹

(The CLAS Collaboration)

¹*Carnegie Mellon University, Pittsburgh, Pennsylvania 15213*

²*Old Dominion University, Norfolk, Virginia 23529*

³*Hampton University, Hampton, Virginia 23668*

⁴*Institut für Kernphysik, Johannes Gutenberg-Universität, 55099 Mainz, Germany*

⁵*Universidad Técnica Federico Santa María, Casilla 110-V Valparaíso, Chile*

⁶*University of Richmond, Richmond, Virginia 23173*

⁷*Ohio State University, Lima, Ohio, 45804*

⁸*Union College, Schenectady, NY 12308*

⁹*Argonne National Laboratory, Argonne, Illinois 60439*

- ¹⁰Arizona State University, Tempe, Arizona 85287-1504
- ¹¹University of California at Los Angeles, Los Angeles, California 90095-1547
- ¹²California State University, Dominguez Hills, Carson, CA 90747
- ¹³Catholic University of America, Washington, D.C. 20064
- ¹⁴CEA-Saclay, Service de Physique Nucléaire, 91191 Gif-sur-Yvette, France
- ¹⁵Christopher Newport University, Newport News, Virginia 23606
- ¹⁶University of Connecticut, Storrs, Connecticut 06269
- ¹⁷Edinburgh University, Edinburgh EH9 3JZ, United Kingdom
- ¹⁸Fairfield University, Fairfield CT 06824
- ¹⁹Florida International University, Miami, Florida 33199
- ²⁰Florida State University, Tallahassee, Florida 32306
- ²¹The George Washington University, Washington, DC 20052
- ²²University of Glasgow, Glasgow G12 8QQ, United Kingdom
- ²³Idaho State University, Pocatello, Idaho 83209
- ²⁴INFN, Laboratori Nazionali di Frascati, 00044 Frascati, Italy
- ²⁵INFN, Sezione di Genova, 16146 Genova, Italy
- ²⁶Institut de Physique Nucleaire ORSAY, Orsay, France
- ²⁷Institute of Theoretical and Experimental Physics, Moscow, 117259, Russia
- ²⁸James Madison University, Harrisonburg, Virginia 22807
- ²⁹Kyungpook National University, Daegu 702-701, Republic of Korea
- ³⁰Massachusetts Institute of Technology, Cambridge, Massachusetts 02139-4307
- ³¹University of Massachusetts, Amherst, Massachusetts 01003
- ³²University of New Hampshire, Durham, New Hampshire 03824-3568
- ³³Norfolk State University, Norfolk, Virginia 23504
- ³⁴Ohio University, Athens, Ohio 45701
- ³⁵University of Pittsburgh, Pittsburgh, Pennsylvania 15260
- ³⁶Rensselaer Polytechnic Institute, Troy, New York 12180-3590
- ³⁷Rice University, Houston, Texas 77005-1892
- ³⁸Skobeltsyn Nuclear Physics Institute, Skobeltsyn
Nuclear Physics Institute, 119899 Moscow, Russia
- ³⁹University of South Carolina, Columbia, South Carolina 29208
- ⁴⁰Thomas Jefferson National Accelerator Facility, Newport News, Virginia 23606

⁴¹ *Virginia Polytechnic Institute and State University, Blacksburg, Virginia 24061-0435*

⁴² *University of Virginia, Charlottesville, Virginia 22901*

⁴³ *College of William and Mary, Williamsburg, Virginia 23187-8795*

⁴⁴ *Yerevan Physics Institute, 375036 Yerevan, Armenia*

⁴⁵ *George Mason University, Fairfax, Virginia 22030*

(Dated: November 11, 2008)

Abstract

The neutron elastic magnetic form factor G_M^n has been extracted from quasielastic electron scattering data on deuterium with the CEBAF Large Acceptance Spectrometer (CLAS) at Jefferson Lab. The kinematic coverage of the measurement is continuous from $Q^2=1$ GeV² to 4.8 GeV². High precision was achieved by employing a ratio technique in which many uncertainties cancel, and by a simultaneous in-situ calibration of the neutron detection efficiency, the largest correction to the data. Neutrons were detected using the CLAS electromagnetic calorimeters and the time-of-flight scintillators. Data were taken at two different electron beam energies, allowing up to four semi-independent measurements of G_M^n to be made at each value of Q^2 . The dipole parameterization is found to provide a good description of the data over the measured Q^2 range.

PACS numbers: 14.20.Dh, 13.40.Gp

The elastic electromagnetic form factors of the proton and neutron are fundamental quantities related to their spatial charge and current distributions. The dominant features of the larger form factors G_M^p , G_E^p , and G_M^n were established in the 1960's: the dipole form $G_D = (1 + Q^2/\Lambda)^{-2}$ where $\Lambda = 0.71 \text{ GeV}^2$ gave a good description of these form factors ($G_M^p/\mu_p \approx G_M^n/\mu_n \approx G_E^p \approx G_D$) within experimental uncertainties, corresponding (at least for $Q^2 \ll 1 \text{ GeV}^2$ or large radii) to an exponential falloff in the spatial densities of charge and magnetization. More recent Jefferson Lab results on the proton form factors show a dramatic departure from the dipole form even at moderate Q^2 [1] while the magnetic form factor of the neutron G_M^n falls below the dipole form at high Q^2 (e.g., $G_M^n/\mu_n G_D = 0.62 \pm 0.15$ at $Q^2 = 10 \text{ GeV}^2$ [2]). Obtaining higher precision measurements of these quantities has been one thrust of the field, while new directions have emerged recently. These include precise measurements of the neutron electric form factor [3], strange electric and magnetic form factors of the proton [4], and time-like form factors [5].

In addition to experimental progress, there has been renewed theoretical interest [6]. First, models of the nucleon ground state can be used to predict these quantities, and so far describing all the modern results has been a challenge [7, 8, 9, 10]. Second, lattice calculations are now becoming feasible in the few-GeV² range, and over the next decade these calculations will become increasingly precise [11]. Finally, elastic form factors are a limiting case related to the zeroth moment of the generalized parton distributions (GPDs) and can be used to constrain GPD models [8]. We also note that some of the models mentioned above and others predict significant deviations from the dipole form for $Q^2 < 5 \text{ GeV}^2$ [9, 11].

To distinguish among these different physics models, high precision and large Q^2 coverage are important. At present the neutron magnetic form factor at larger Q^2 is known much more poorly than the proton form factors [6]. In this Letter we report on a new measurement of G_M^n in the range $Q^2 = 1.0 - 4.8 \text{ GeV}^2$ at Jefferson Lab. The precision and coverage of these results eclipse the world's data on this elastic form factor in this Q^2 range. Systematic uncertainties were held to 3% or less.

In the absence of a free neutron target, we measure the ratio R of the cross sections for the ${}^2\text{H}(e, e'n)p$ and ${}^2\text{H}(e, e'p)n$ reactions in quasielastic (QE) scattering on deuterium. The notation ${}^2\text{H}(e, e'n)p$ (${}^2\text{H}(e, e'p)n$) indicates that a neutron (proton) with most of the momentum from the scattered electron is detected in coincidence with the final state electron.

The ratio R is defined as $R = \frac{d\sigma}{d\Omega}[{}^2\text{H}(e, e'n)_{QE}]/\frac{d\sigma}{d\Omega}[{}^2\text{H}(e, e'p)_{QE}]$ [12, 13, 14, 15] and

$$R = a(E, Q^2, \theta_{pq}^{max}, W_{max}^2) \times \frac{\sigma_{Mott} \left(\frac{(G_E^n)^2 + \tau(G_M^n)^2}{1 + \tau} + 2\tau \tan^2 \frac{\theta}{2} (G_M^n)^2 \right)}{\frac{d\sigma}{d\Omega}[{}^1\text{H}(e, e')p]}, \quad (1)$$

where E is the beam energy, σ_{Mott} is the cross section for scattering off a point particle of unit charge, $\tau = Q^2/4M^2$, M is the nucleon mass, and θ is the electron scattering angle. The factor $a(E, Q^2, \theta_{pq}^{max}, W_{max}^2)$ corrects for nuclear effects and depends on E and cuts on θ_{pq}^{max} , the maximum angle between the nucleon direction and the three-momentum transfer \vec{q} , and W_{max}^2 , the maximum value of the mass recoiling against the electron assuming the target was at rest. We have used the one-photon exchange approximation in the numerator of Eq. 1 to express the cross section in terms of the neutron form factors. The right-hand side of Eq. 1 contains the desired G_M^n along with the much-better-known proton cross section and the neutron electric form factor (G_E^n), which is small over the Q^2 range studied here. For QE kinematics (within a cone θ_{pq}^{max} around \vec{q}) G_M^n can be extracted from Eq. 1 as a function of Q^2 by relying on knowledge of the proton cross section and G_E^n , accurate calculations of $a(E, Q^2, \theta_{pq}^{max}, W_{max}^2)$, and precise measurements of R . The ratio method has the added benefit that it is less vulnerable to nuclear structure (*e.g.*, choice of deuteron wave function, final-state interactions, *etc.*) [13] and experimental effects (*e.g.*, radiative corrections, luminosity, *etc.*). The challenge here is to accurately measure the nucleon detection efficiencies.

The two reactions were measured in the CLAS detector [16] at the same time and from the same target to reduce systematic uncertainties. Two electron-beam energies were used, 2.6 GeV and 4.2 GeV. CLAS consists of six independent magnetic spectrometers each instrumented with drift chambers [17], time-of-flight (TOF) scintillators covering polar angles $8^\circ < \theta < 143^\circ$ [18], a gas-filled threshold Cherenkov counter (CC) [19], and a lead-scintillator sandwich-type electromagnetic calorimeter (EC) covering $8^\circ < \theta < 45^\circ$ [20]. CLAS was triggered on electrons by requiring a coincidence between CC and EC signals in one sector. Neutrons were measured separately in the TOF and EC while protons were measured using the drift chambers and TOF systems. A novel dual-cell target was used consisting of two collinear cells each 6-cm long - one filled with ${}^1\text{H}$ and the other with ${}^2\text{H}$ - and separated by 4.7 cm. The downstream cell was filled with liquid hydrogen for calibrations and efficiency

measurements. The upstream cell was filled with liquid deuterium for the ratio measurement. The target was made of aluminum with 20-micron aluminum windows. The CLAS vertex resolution of 2 mm enabled us to distinguish between events from the different targets [16].

We now describe the analysis including corrections to R . Nucleons from quasielastic events tend to be ejected close to the direction of the 3-momentum transfer while inelastically scattered nucleons are not [13]. We required the angle θ_{pq} between the nucleon 3-momentum and the 3-momentum transfer to be small ($\theta_{pq}^{max} = 2.5^\circ - 4.5^\circ$ across the Q^2 range) and integrated over all azimuthal angles about the 3-momentum transfer. Another cut, $W^2 < W_{max}^2 = 1.2 \text{ GeV}^2$ eliminated most inelastic events that survived the θ_{pq}^{max} cut. Our simulations of the inelastic [21] and quasielastic production [12], which include the effects of Fermi motion in the target show the fraction of inelastic events surviving these cuts is less than 0.5% of the total. To measure R accurately, the solid angles of CLAS for neutrons and protons have to be identical. The nucleon solid angles were matched by first determining event-by-event the nucleon momentum from the electron kinematics under the assumption of quasielastic scattering. The expected proton and neutron trajectories in CLAS were checked to see if both trajectories would lie within the CLAS acceptance. Only the events where both nucleons were expected to strike the active area of CLAS were analyzed.

Once the event sample was selected, corrections for the detector efficiencies, Fermi motion, and other effects were applied. Neutrons were measured in two CLAS scintillator-based detectors: the EC and the TOF. The neutron detection efficiency (NDE) measurement was performed using tagged neutrons from the $^1\text{H}(e, e'\pi^+)n$ reaction, where the mass of the unobserved neutron was inferred from the measured electron and pion kinematics and matched with possible hits in the neutron detector. Since the precise value of the detection efficiency can vary with time-dependent and rate-dependent quantities such as photomultiplier tube gain, the detection efficiency was measured *simultaneously* with the primary deuterium measurement. The measured neutron detection efficiency for each sector for the TOF and for nine sections in each EC sector were fitted with polynomials at low neutron momenta and a constant at high momenta. Plots of NDE integrated over all CLAS angles are shown in Fig. 1. The different sets of points correspond to beam energies of 2.6 GeV (red triangles) and 4.2 GeV (black squares). For both detection systems the agreement between the two

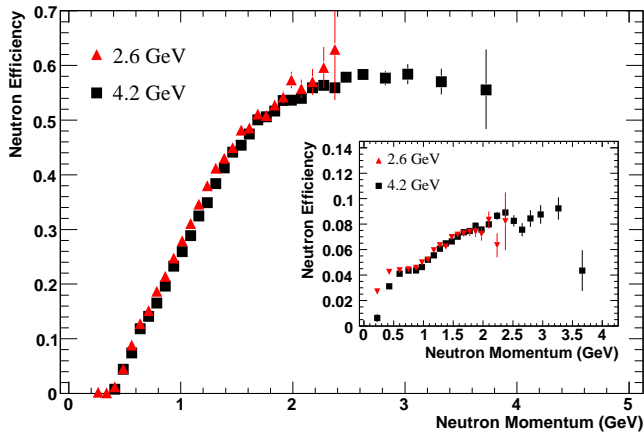


FIG. 1: (color online). Detection efficiency versus neutron momentum detected in the EC (main panel) and in the TOF system (inset) at two beam energies. For R the neutron momentum was > 1.0 GeV.

beam energies is excellent and the uncertainty is small over a broad neutron momentum range. The calibration target was also used to measure the proton detection efficiency using elastic scattering $p(e, e'p)$. The kinematics of the scattered electron were used to predict the location of the elastically scattered proton in CLAS and the event was searched for a proton at that location.

The nuclear correction factor, $a(E, Q^2, \theta_{pq}^{max}, W_{max}^2)$, in Eq. 1 was calculated by Jeschonek using the procedure described in Ref. [22]. A calculation of the cross section was performed using the Plane Wave Impulse Approximation (PWIA) for $Q^2 \geq 1.0$ GeV² and the AV18 deuteron wave function [23]. Final state interactions (FSI) were included using Glauber theory and the correction calculated as the ratio of the full calculation including FSI to the PWIA without FSI. The final correction applied to R was averaged over the same θ_{pq} range used in the analysis. This nuclear correction to R was less than 0.1% across the full Q^2 range.

In our analysis we assumed QE kinematics and ignored the Fermi motion that can knock the ejected nucleon out of the CLAS acceptance. To correct for this effect we simulated quasielastic scattering from a fixed target nucleon and tested to see if it struck the active area of CLAS (an expected event). We then simulated the nucleon's internal motion (using the Hulthen distribution) and elastic scattering from this moving particle. Using the target momentum (known in the simulation) we re-calculated the trajectory to see if it still struck

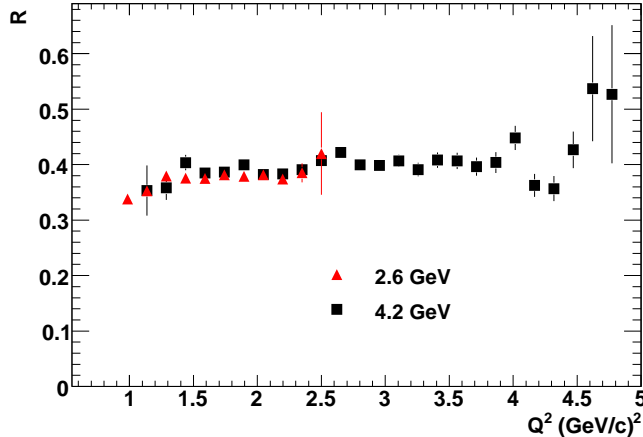


FIG. 2: (color online). Results for the ratio of $e - n/e - p$ events (R) as a function of Q^2 for two beam energies. Each set is a weighted sum of the TOF and EC neutron measurements. Only statistical uncertainties are shown. Numerical results are reported in the CLAS Physics Data Base [24].

CLAS and satisfied the θ_{pq}^{max} cut (an actual event). The ratio of actual to expected events is the correction factor for that nucleon. The ratio of these corrections for the neutron and the proton multiplies R . The correction to G_M^n is in the range $\approx 0.9 - 1.3$.

We present our results for the ratio R in Fig. 2 for the two beam energies. The corrections described above have been included and only statistical uncertainties are shown. For each beam energy in Fig. 2 we averaged the results for the two neutron measurements (EC and TOF) weighted by the statistical uncertainties. Note that measurements of R at the same Q^2 but different beam energies are not expected to be the same because the kinematics are not the same (recall Eq. 1). The data cover the Q^2 range with excellent statistical accuracy and with a large overlap between the two data sets.

A detailed study of each correction's contribution to the systematic uncertainty has been made [12]. Listed in Table I are the largest contributions to this systematic uncertainty along with the maximum (typical) value across the full Q^2 range. The largest contributions come from the parameterizations of the neutron detection efficiencies for the TOF and EC systems. To estimate the uncertainty associated with the NDE measurement, the order of the polynomial and position of the edge of the constant region used to fit the data were varied to determine the effect on G_M^n as a function of Q^2 . Uncertainties were in the range

0.5-3.2%.

The extraction of G_M^n from R depends on the other elastic form factors (see Eq. 1) and their uncertainties contribute to the uncertainty in G_M^n . The uncertainty in the proton cross section was estimated using the difference between two parameterizations by Bosted and Arrington [25, 26]. The average difference was less than 1% with a maximum of 1.5%. For the effect of G_E^n , the difference between the Galster parameterization and a fit by Lomon was used [27, 28] and a maximum uncertainty of 0.7% was obtained. The upper limit of the θ_{pq} cut was varied by $\pm 10\%$, changing G_M^n by a maximum of about 0.5% and by 0.3% on average [12]. The systematic uncertainty associated with the Fermi motion correction was calculated using two dramatically different choices for the Fermi momentum distribution of the deuteron: a flat distribution and the Hulthen distribution. This correction to G_M^n changes by less than 1% between the two Fermi motion distributions. The quadrature sum of the remaining, maximum systematic uncertainties was less than 0.5% [12]. The final systematic uncertainty for the EC measurement was less than 2.4% and for the TOF measurement it was less than 3.6%

As mentioned above, the CLAS extraction of $G_M^n(Q^2)$ consists of overlapping measurements. The TOF scintillators cover the full angular range of CLAS, while the EC system covers a subset of these angles, so G_M^n can be obtained from two independent measurements of the $e - n$ production. In addition, the experiment was performed with two different beam energies with overlapping Q^2 coverage so the detection of the protons and neutrons of a given Q^2 took place in two different regions of CLAS. Essentially four measurements of G_M^n have been obtained from the CLAS data that could have four semi-independent sets of systematic uncertainties. Shown in Fig. 3 are the results for G_M^n from the different measurements divided by $\mu_n G_D$ for normalization and to reduce the dominant Q^2 dependence. Only

Quantity	$\delta G_M^n / G_M^n$	Quantity	$\delta G_M^n / G_M^n$
EC NDE	< 1.5% (1%)	TOF NDE	< 3.2% (2%)
proton σ	< 1.5% (0.8%)	G_E^n	< 0.7% (0.5%)
Fermi loss	< 0.9% (0.5%)	θ_{pq} cut	< 1.0% (0.3%)
Remainder	< 0.5% (0.2%)		

TABLE I: Upper limits (typical values) of the estimated systematic errors.

statistical uncertainties are shown. Here the different measurements should agree because G_M^n depends only on Q^2 . The two measurements for each beam energy are consistent within the statistical uncertainties, suggesting the systematic uncertainties for the EC and SC are well-controlled and small.

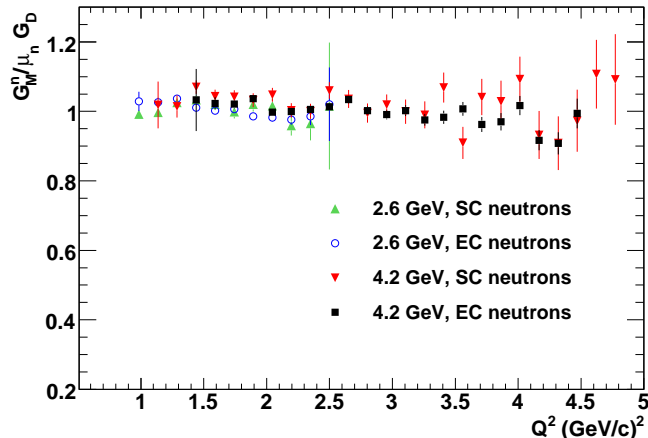


FIG. 3: (color online). Results for $G_M^n/(\mu_n G_D)$ as a function of Q^2 for four different measurements (two beam energies). Only statistical uncertainties are shown.

The results in Fig. 3 were then combined in a weighted average as a function of Q^2 . The final systematic uncertainty varied from 1.7-2.5% across the full data range. Note that the larger uncertainty on the parameterization of the TOF neutron detection efficiency (see Table 1) did not push the total, weighted uncertainty above our goal of 3%. There are considerably more calorimeter data due to its higher efficiency (see Fig. 1) and the maximum EC uncertainty was 1.5% [12].

The final, combined results for the neutron magnetic form factor are shown in Fig. 4 together with a sample of existing data [6, 29]. The uncertainties shown are statistical only. Systematic uncertainties are represented by the band below the data. A few features are noteworthy. First, the quality and coverage of the data is a dramatic improvement of the world's data set. Second, our results are consistent with that previous data, but with much smaller uncertainties. Third, the dipole form is a good representation of the data here, which differs from parameterizations and some calculations at higher Q^2 where previous data for $G_M^n/(\mu_n G_D)$ decrease with increasing Q^2 [6, 9, 11]. We also note any fluctuations in our results (*e.g.* at 1.29 GeV²) are not significant enough for us to draw any firm conclusions here.

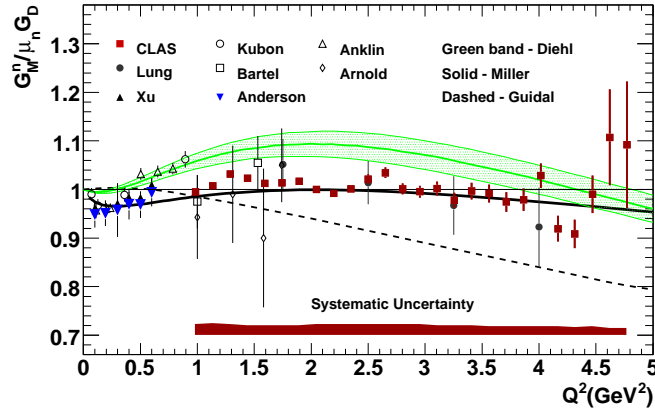


FIG. 4: (color online). Results for $G_M^n/(\mu_n G_D)$ from the CLAS measurement are compared with a selection of previous data [14, 29, 31, 32, 33, 34, 35] and theoretical calculations [7, 8, 9, 30]. Numerical results are reported in the CLAS Physics Data Base [24].

The curves shown in Fig. 4 are from Diehl *et al.* [8], Guidal *et al.* [9], and Miller *et al.* [7, 30] and are all constrained by the world's previous data. In Diehl *et al.* the GPDs are parameterized and fitted to the experimental data (green band). The curve reproduces some of the low- Q^2 data, but lies above our results. Guidal *et al.* use a Regge parameterization of the GPDs to characterize the elastic nucleon form factors at low momentum transfer and extend it to higher Q^2 (dashed line). The curve reproduces the existing, higher Q^2 data, but is not consistent with our results. In the calculation of Miller *et al.*, the nucleon is treated using light-front dynamics as a relativistic system of three bound quarks and a surrounding pion cloud (solid curve). The model achieves a good description of much of the previous nucleon form factor data even at high Q^2 and is consistent with our results.

In summary, the neutron magnetic form factor G_M^n has been measured in the range $Q^2 = 1.0 - 4.8 \text{ GeV}^2$ with systematic uncertainties less than 2.5%. The measurements were made with the CLAS detector at Jefferson Lab at two incident beam energies using the ratio of $e - n$ to $e - p$ scattering. Neutrons were measured with two independent systems: time-of-flight scintillators and electromagnetic calorimeters. Detector efficiencies were measured with a dual-cell target containing ^2H and ^1H so the efficiencies were measured simultaneously with the production data. The data are a significant improvement in precision and coverage in this Q^2 range and are surprisingly consistent with the long-established dipole form. The

calculation by Miller *et al.* is in good agreement with our results.

We acknowledge the outstanding efforts of the staff of the Accelerator and the Physics Divisions at Jefferson Lab that made this experiment possible. This work was supported in part by the Italian Istituto Nazionale di Fisica Nucleare, the French Centre National de la Recherche Scientifique and Commissariat à l’Energie Atomique, the U.S. Department of Energy, the National Science Foundation, an Emmy Noether grant from the Deutsche Forschungsgemeinschaft, the U.K. Engineering and Physical Science Research Council, and the Korean Science and Engineering Foundation. Jefferson Science Associates (JSA) operates the Thomas Jefferson National Accelerator Facility for the United States Department of Energy under contract DE-AC05-06OR23177.

* Current address: Kyungpook National University, Daegu 702-701, Republic of Korea

† Current address: Ohio University, Athens, Ohio 45701

‡ Current address: Systems Planning and Analysis, Alexandria, Virginia 22311

§ Current address: Thomas Jefferson National Accelerator Facility, Newport News, Virginia 23606

¶ Current address: Los Alamos National Laboratory, New Mexico, NM

** Current address: Catholic University of America, Washington, D.C. 20064

†† Current address: The George Washington University, Washington, DC 20052

‡‡ Current address: Christopher Newport University, Newport News, Virginia 23606

§§ Current address: Edinburgh University, Edinburgh EH9 3JZ, United Kingdom

[1] O. Gayou *et al.*, Phys. Rev. Lett. **88**, 092301 (2002).

[2] S. Rock *et al.*, Phys. Rev. Lett. **49**, 1139 (1982).

[3] R. Madey *et al.*, Phys. Rev. Lett. **91**, 122002 (2003).

[4] K. A. Aniol *et al.*, Phys. Lett. B **365**, 275 (2006).

[5] F. Iachello and Q. Wan, Phys. Rev. C **69**, 055204 (2004).

[6] C. Hyde-Wright and K. deJager, Ann. Rev. Nucl. Part. Sci. **54**, 217 (2004).

[7] G.A. Miller, Phys. Rev. C **66**, 032201(R) (2002).

[8] M. Diehl *et al.*, Eur. Phys. J. C **39**, 1 (2005).

[9] M. Guidal *et al.*, Phys. Rev. D **72**, 054013 (2005).

- [10] M. A. Belushkin *et al.*, Phys. Rev. C **75**, 035202 (2007).
- [11] J. Ashley *et al.*, Eur. Phys. J A **19**, 9 (2004).
- [12] J. D. Lachniet, Ph.D. thesis, Carnegie-Mellon University, Pittsburgh, PA, USA (2005).
- [13] L. Durand, Phys. Rev. **115**, 1020 (1959).
- [14] W. Bartel *et al.*, Nucl. Phys. B **58**, 429 (1973).
- [15] H. Anklin *et al.*, Phys. Lett. B **428**, 248 (1998).
- [16] B. A. Mecking *et al.* (CLAS), Nucl. Instrum. Meth. A **503**, 513 (2003).
- [17] M. Mestayer *et al.*, Nucl. Inst. and Meth. A **449**, 81 (2000).
- [18] E. Smith *et al.*, Nucl. Inst. and Meth. A **432**, 265 (1999).
- [19] G. Adams *et al.*, Nucl. Inst. and Meth. A **465**, 414 (2001).
- [20] M. Amarian *et al.*, Nucl. Inst. and Meth. A **460**, 239 (2001).
- [21] P. Corvisiero *et al.*, Nucl. Instr. and Meth. **A346**, 433 (1994).
- [22] S. Jeschonnek *et al.*, Phys. Rev. C **62**, 044613 (2000).
- [23] R.B. Wiringa *et al.*, Phys. Rev. C **51**, 38 (1995).
- [24] URL <http://clasweb.jlab.org/physicsdb>.
- [25] P.E. Bosted, Phys. Rev. C **51**, 409 (1995).
- [26] J. Arrington, Phys. Rev. C **68**, 034325 (2003).
- [27] S. Galster *et al.*, Nucl. Phys. B **32**, 221 (1971).
- [28] E.L. Lomon, Phys. Rev. C **66**, 045501 (2002).
- [29] B. Anderson *et al.*, Phys. Rev. C **75**, 034003 (2007).
- [30] H. Matevosyan *et al.*, Phys. Rev. C **71**, 055204 (2005).
- [31] G. Kubon *et al.*, Phys. Lett. B **524**, 26 (2002).
- [32] A. Lung *et al.*, Phys. Rev. Lett. **70**, 718 (1993).
- [33] H. Anklin *et al.*, Phys. Lett. B **336**, 313 (1994).
- [34] R. G. Arnold *et al.*, Phys. Rev. Lett. **61**, 806 (1988).
- [35] W. Xu *et al.*, Phys. Rev. C **67**, 012201 (2003).